PCCP

Accepted Manuscript

ROYAL SOCIETY OF CHEMISTRY

www.rsc.org/pccp

Journal Name

RSCPublishing

ARTICLE

Origin of surface trap states in CdS quantum dots: Relationship between size dependent photoluminescence and sulfur vacancy trap states

Cite this: DOI: 10.1039/xoxxoooooox

Received ooth January 2012,
Accepted ooth January 2012

DOI: 10.1039/xoxxoooooox

www.rsc.org/

Aisea Veamatahau,[a] Bo Jiang,[a] Tom Seifert,[a†] Satoshi Makuta,[a] Kay Latham,[b] Masayuki Kanehara,[c] Toshiharu Teranishi,[d] and Yasuhiro Tachibana*[aef]

Monodisperse cadmium sulphide (CdS) quantum dots (QDs) with a tunable size from 1.4 to 4.3 nm were synthesized by a non-injection method, and their surface states were characterized by photoluminescence spectroscopy and X-ray Photoelectron Spectroscopy (XPS). The steady state photoluminescence study identified that the proportion of the trap state emission increased with the QD size decrease, while from the photoluminescence decay study, it appeared that the trap state emission results from the emission via a surface deep trap state. The XPS measurements revealed the existence of surface Cd with sulfur vacancy sites which act as electron trap sites, and the population of these sites increases with the QD size decrease. These results are consistent to conclude that the trap state emission mainly originates from the surface deep trapped electrons at the surface Cd with sulfur vacancy sites.

Introduction

Semiconductor quantum dots (QDs) have received significant interest owing to their versatile characteristics, such as high photoluminescence quantum yield,[1-3] a wide light absorption wavelength range[4-6] and their size dependence on absorption and emission profiles, originating from "quantum size confinement".[7-10] Application of QDs to solar energy conversion devices requires an understanding of relaxation pathways of photoexcited QDs[11-13] and of charge separated states.[14] QDs are assembled and attached to other semiconductors or metals directly or through surface binding molecules. QD surface modification often creates surface or interfacial trap states that reduce the number of exciton states or energy through (non)radiative charge recombination. To minimize such trap states, QDs are typically coated by a ligand or a shell, in particular thicker shells are known to improve photoluminescence quantum yields.[15-17] However, the thicker shells may isolate a core exciton state, and even diminish the interaction between an exciton state and other materials which receive an electron or hole from the core state.[18] Understanding the interaction of the photoexcited QD with surface traps, coordinating ligands, solvents and electron donor/acceptors is not therefore trivial in the construction and design of efficient energy conversion devices.[19, 20]

Among the large number of different types of QDs, metal chalcogenide QDs, e.g. CdS and CdSe QDs, have most commonly been studied owing to their ease of synthesis and distinctive optical properties.[12, 21-23] Steady state and time-resolved photoluminescence spectroscopies have often been employed to characterize the excited state structure of CdS QDs over the last three decades.[24-31] While the exciton state photoluminescence has been characterized, the origin of trap state emission is not well understood. Brus and McLendon mainly focused on characterizing trap state photoluminescence, and concluded that the photoluminescence is attributed to charge recombination between a trapped electron and a trapped hole at the QD surface.[26, 30] However, no detailed study has been conducted to clarify the relationship between CdS QD surface structure and trap state photoluminescence.

In this paper, we demonstrate characterization of trap states of CdS QDs with a series of sizes using optical spectroscopies such as photoluminescence spectroscopies and X-ray Photoelectron Spectroscopy (XPS). A wide variety of CdS QDs were synthesized by employing a non-injection synthesis method. Recently, Teranishi et al. has reported a non-injection synthesis of high quality CdS and Cu_7S_4 QDs.[32] This study has motivated us to investigate synthesis conditions in detail to extend the ability to control QD size over a wider range and their size distribution. We have investigated size dependent photoluminescence with comparison between exciton and trap states, and have correlated the trap state photoluminescence with QD surface structures identified by XPS measurements.

Experimental

Chemicals

Cadmium stearate (>85.0 % pure) and 1,3-dibutyl-2-thiourea (>95.0 % pure) were purchased from Wako Pure Chemical Industries, Ltd., Japan. Oleylamine (70% pure) was purchased from Sigma-Aldrich Co. LLC. Bulk CdS powder (LR grade) was purchased from BDH. Di-n-octyl ether (>95.0 % pure) was purchased from Tokyo Chemical Industry Co., Ltd., Japan. All of these chemicals were used without further purification.

Non-injection synthesis of CdS QDs

Zinc blende CdS QDs with a narrow size distribution were synthesized by a non-injection method, similar to the procedure reported previously.[32] Cadmium stearate (0.3 mmol), oleylamine (3.0 mmol) and 1,3-dibutyl-2-thiourea (0.15 mmol) were dispersed in 9 mL of di-n-octyl ether (Cd:S = 2:1). Oxygen and water were removed from the solution under vacuum at room temperature, and subsequently the solution was heated to 90~210 ºC under nitrogen atmosphere, forming CdS QDs. After the solution was cooled to room temperature, the synthesized QDs were purified with methanol, and subsequently acetone to remove excess ligands, unreacted precursors or by-products. The purified QDs were dissolved in chloroform without size sorting. QD sizes of <3.2 nm were obtained by adjusting the heating temperature between 90 and 210 ºC, and the heating time.

QD sizes greater than 3.2 nm were prepared simply by adding the same amount of precursors into the synthesized QD solution without purification, and by conducting the reaction at 210~250 ºC. When necessary, the precursor addition and the reaction were repeated to further grow the QD size. For example, QD sizes of 3.3 nm, 3.7 nm and 4.3 nm were obtained by repeating the reaction: twice at 210 ºC, three times at 250 ºC, and five times at 250 ºC, respectively. After the final reaction, the synthesized QDs were purified with methanol, and subsequently acetone, and finally the QDs were dissolved in chloroform.

Electron microscopy measurements

Electron microscopy images of the synthesized QDs were obtained by Hitachi H-9000NAR transmission electron microscopy (TEM) operated at 300 kV at the Research Center for Ultra-High Voltage Electron Microscopy in Osaka University, or by JEOL 2010 transmission electron microscopy operated at 200 kV at RMIT Microscopy and Microanalysis Facility (RMMF) in RMIT University. The samples were prepared by casting a drop of diluted QD solutions onto a 300-copper mesh grid coated by a carbon film, followed by drying them in air at room temperature.

XRD measurements

X-ray diffraction patterns were obtained by a Bruker D8 Discover microdiffractometer fitted with a GADDS (General Area Detector Diffraction System). Data was collected at room temperature using Cu Kα radiation (λ = 1.54178 Å) with a potential of 40 kV and a current of 40 mA, and filtered with a graphite monochromator in parallel mode (175 mm collimator with 0.5 mm pinholes). The samples were prepared by casting a drop of QD solutions onto a glass plate, followed by drying them in air at room temperature. The samples were mounted vertically, and aligned on an XYZ stage with the aid of a camera and laser guide.

XPS measurements

X-ray photoelectron spectra were measured at room temperature using an Al *K*-alpha X-ray Photoelectron Spectrometer (Thermo Scientific, *K*-alpha). The samples were prepared by drop-casting QD solution on a silicon wafer. A linear or polynomial background was subtracted prior to peak fitting analysis. The XPS spectrum of the bulk CdS sample was first fitted with a Voigt function. The spectra of CdS QDs were then fitted with a Voigt function, assuming the same line widths as those from the fitting with bulk CdS. This fitting procedure merely influenced peak binding energy positions for all samples. The measured spectra were calibrated using the position of the C 1S peak at 284.6 eV.

Absorption and emission measurements

Steady state absorption spectra were measured by a JASCO-V670 UV-VIS-NIR absorption spectrometer. The purified CdS QD solution was diluted with chloroform to obtain an absorbance of ~0.3 at the first exciton peak in the cuvette with 1 cm optical length. This is equivalent to the concentration of 0.3~0.8 μM.[33]

Steady state photoluminescence (PL) spectra were collected in a 1 x 1 cm^2 quartz glass cuvette with 90º incident excitation using Photon Technology International (PTI) fluorometer with a xenon arc lamp light source at 22 ºC. The spectra were observed using a photomultiplier detector in a wavelength range between 420 and 800 nm with the wavelength resolution of 1.6 nm, and using a thermo-electrically cooled InGaAs detector with a chopper and a lock-in amplifier in a wavelength range between 700 and 1,240 nm with the wavelength resolution of 4 nm. The spectra were corrected for the spectral response of the grating in the emission monochromator and detectors. The influence of an overtone of the excitation wavelength from the monochromators was removed for clarity of the data presentation. Photoluminescence quantum yield (QY) was determined by using an integrating sphere emission collector. The data were collected with a wavelength scanning step of 0.125 nm.

Nanosecond transient photoluminescence decays were measured using a Photon Technology International (PTI) emission spectrometer with a time-resolved stroboscopic detection system. An LED light pulse with a pulse width of 1.5 ns was used to excite the QD solution with the excitation wavelength of 405 nm and the light intensity of 10 pJ/pulse at 25 kHz. The excitation density is extremely small (<< 1 exciton state formed per QD), and thus the exciton-exciton annihilation owing to the trap state saturation was avoided.[34] The detection band width is approximately 24 nm. The instrument response time is 1.5 ns (FWHM) without deconvolution. The CdS QD solution in a 1 x 1 cm^2 quartz glass cuvette was excited at the angle of 90º from the detector plane at 22 ºC. High wavelength

pass filters were used in the emission pathway to remove the scattered excitation light. No change in the steady state absorption and photoluminescence spectra before and after the transient experiments was observed, confirming that the samples were stable during the dynamics measurements.

Results and discussion

CdS QD synthesis

In a non-injection synthesis method, all required precursors are mixed in a container, and the reaction to form nuclei is initiated by increasing the heating temperature. In this case, reaction temperature and heating time largely influence the QD size. A large amount of CdS QDs can be obtained by this method. Although several groups reported non-injection synthesis method, the quality or size tunability is limited, compared to the hot injection method.[35-41]

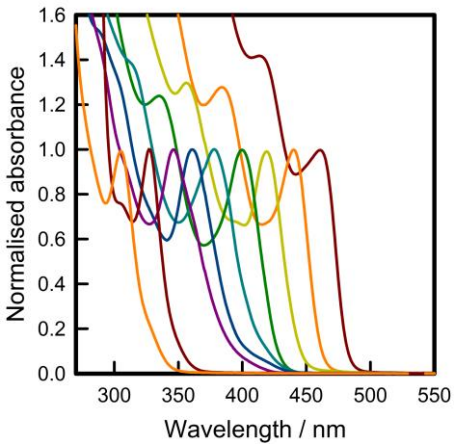

Fig. 1. Absorption spectra of CdS QD with a series of diameters. The first exciton peak wavelength can approximately be tuned to 305, 325, 345, 360, 380, 400, 420, 440 or 460 nm.

In the current study, CdS nucleation started from 90 ºC, which is lower than reported in previous typical CdS QD syntheses.[23, 39, 42] QD size was simply controlled by adjusting the heating temperature between 90 and 210 ºC, and the heating time. Lower heating temperature resulted in smaller size QDs. Fig. 1 shows absorption spectra of various QDs with a size from 1.4 to 4.3 nm. The QD size smaller than 2.5 nm was estimated from the first exciton peak position of the absorption spectrum, following the report published by Peng et al.,[33] while the TEM images were used to determine the QD size greater than 2.5 nm. The spectra were normalised at the first exciton peak position. Distinctive 2nd exciton peaks were also observed over UV and visible wavelengths, indicative of a narrow size distribution in each QD solution.[23, 39] The smallest size of 1.4 nm (magic sized nanocluster),[23] estimated from the report published by Peng et al.,[33] with the exciton peak of 305 nm, were synthesized by heating the precursor solution at 90 °C for 1 hour. The heating temperature of 110, 130, 150, 170 or 190 °C for 3 hours, resulted in a first exciton peak at 327, 346, 361, 378 or 400 nm, respectively. As the QD size increases, the first exciton peak position shifts to a longer wavelength in agreement with the "quantum size effect".[23] These observations imply that the QD growth stage can be separated from the nucleation stage. Moreover, we did not observe any detectable new nucleation during the QD growth. Note that QD sizes greater than 3.2 nm were synthesized by adding the same amount of precursors into the synthesized QD solution without purification and repeating the process with reaction temperature of 210~250 ºC (see Experimental for the details). In this non-injection synthesis, the QD size distribution is extremely sensitive to the type of precursor, ligand, solvent and atmosphere. For example, employing octadecylamine, sulfur or diphenyl ether instead of oleylamine, 1,3-dibutyl-2-thiourea or n-octyl ether, respectively, did not result in narrower size distributions, as shown in Fig. S2 in the Electronic Supplementary Information. Water or oxygen contamination increased size distribution.

TEM measurements and analysis were performed to characterize the synthesized CdS QDs. Fig. 2a shows a TEM image of the purified CdS QD (without size sorting) prepared by repeating the growth process three times. Despite the repeated processes, this image shows close-packed arrays with a uniform size distribution. The QD size was analysed by observing the diameter of each nanoparticle. Fig. 2b shows the size histogram of these QDs with an average diameter of 4.1 nm and a standard deviation of 0.40 nm. Fig. 2c shows a high-resolution image of a single QD (4.0 nm), in which clear lattice fringes are seen throughout the dot with a d-spacing of 3.33 Å. This lattice spacing indicates (111) lattice plane of the CdS cubic (zinc blende) crystal structure. Fig. 2d shows a Selected Area Electron Diffraction (SAED) pattern, where agglomerates of QDs were formed. This pattern also matched with that of CdS zinc blende crystal structure.[43, 44] The zinc blende structure was also obtained by others employing similar non-injection synthesis methods[39] or the injection method.[45]

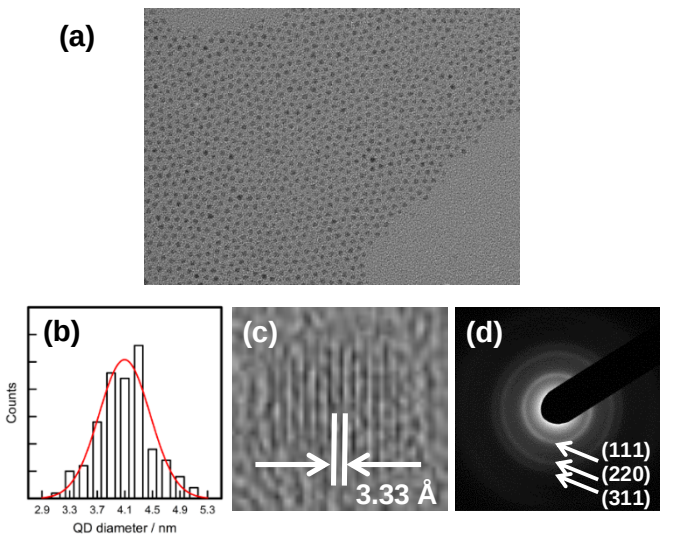

Fig. 2. (a) TEM image of CdS QDs with an average diameter of 4.1 nm. (b) A histogram of QD size. The red solid line shows Gaussian fitting with a distribution of 10 %. (c) HRTEM image of a single 4.0 nm QD. (d) An electron diffraction pattern of CdS QDs. The relevant planes are indexed in the figure.

TEM measurements were also conducted for samples with different sizes. Fig. S3 in the Electronic Supplementary Information shows TEM images and size histograms of the QDs with an average diameter of 3.1, 3.3, 3.7 and 4.3 nm. Although lattice fringes were not clear for smaller QDs, the SAED patterns of all samples indicated a zinc blende structure. Therefore, the zinc blende crystal structure appears to be independent of QD size or synthesis process repetition, even though the heating temperature was raised to 250 °C at the maximum.

XRD measurements were performed for the QDs, and a typical example for the QD with the average diameter of 4.3 nm is shown in Fig. 3. The pattern indicates an excellent match with that of CdS zinc blende structure (ICDD card No. 65-2887). A broadening of reflection peaks at (111), (220) and (311) planes is clearly observed, indicative of small crystallinity size. The mean crystalline diameter was calculated, by fitting the line-width of the main (111) reflection at 2θ of 26.4º with a Gaussian function, using the Debye-Scherrer formula, resulting in 3.1 nm. The sizes estimated from XRD measurements appeared to be smaller than those obtained from TEM measurements.

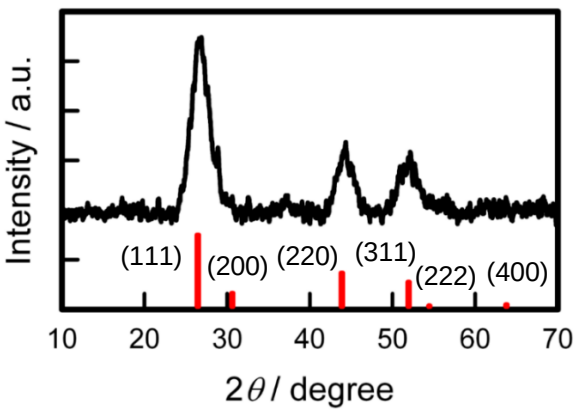

Fig. 3. X-ray diffraction pattern of CdS QD (4.3 nm). The vertical lines at the bottom indicate CdS zinc blende structure pattern (ICDD card No. 65-2887) with the lattice plane index.

QD size dependence on photoluminescence

Optical characterization of the synthesized QDs was performed. The absorption and emission spectra for QDs with a diameter of 3.1, 3.3, 3.7 and 4.3 nm are shown in Fig. 4. In addition to the indicative absorption peaks, photoluminescence spectra indicate two peaks. The higher energy narrow band is assigned to band edge emission, while the other lower energy broad band originates from trap states.[26, 30, 42] Interestingly, compared to most previous studies,[26, 29, 42, 46] the lower energy band is broader with the emission onset at 1,000~1,200 nm. This observation is similar to that reported by Weller et al,[31] who synthesized CdS QDs in aqueous phase, and thus the trap states with a wide range of energy levels are probably irrelevant to the solvent employed for the synthesis. The peak energy (wavelength) of the first exciton absorption ($1S_e$-$1S_h$ transition), and the band edge and trap-state emission peak positions are summarized in Table 1. Note the bulk band gap for zinc blende CdS is 2.42 eV.[47] Similar to the first exciton absorption peak shift, the band edge and trap state emission peaks also shift to longer wavelength, as the QD size increases. These two emission bands were analysed by fitting with a Gaussian distribution function. The fitted data are shown as dotted lines in Fig. 4. Clear fitting results indicate a Gaussian distribution of the trap states. Table 1 also summarizes the fitted FWHM for each band. Clearly the band width becomes narrower with increase in QD size.

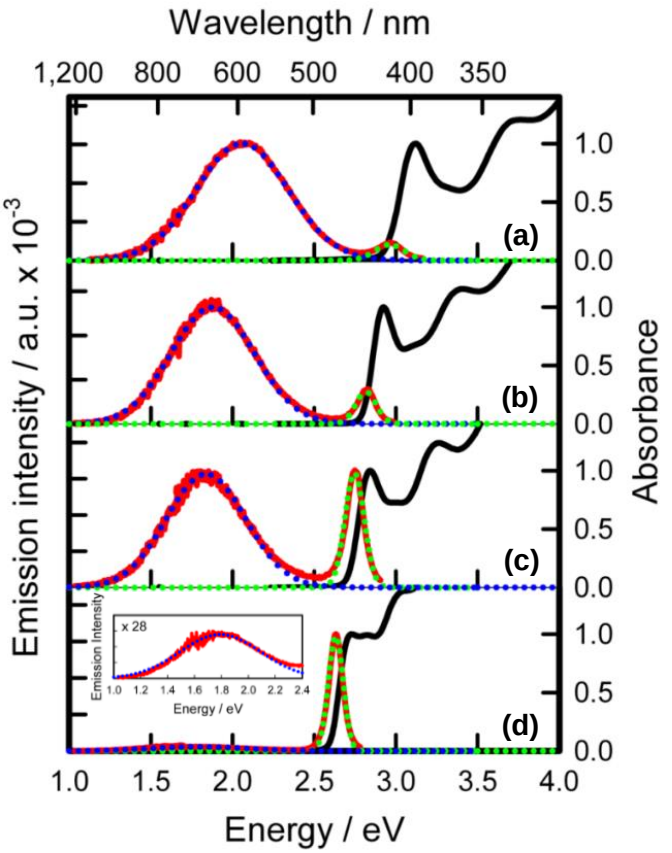

Fig. 4. Steady state absorption (black solid line) and photoluminescence (red solid line) spectra of CdS QDs with a diameter of (a) 3.1 nm, (b) 3.3 nm, (c) 3.7 nm and (d) 4.3 nm. The absorption spectra were normalized at the first exciton peak. The photoluminescence spectra were normalized at the maximal amplitude, either at a band edge or a trap state emission. Inset: magnified trap state emission of QDs (4.3 nm). The band edge (green dotted line) and trap state (blue dotted line) emission data were fitted with a Gaussian distribution function.

Table 1. CdS QD sizes determined from TEM measurements. Their respective absorption and emission peak positions, and FWHMs fitted from the photoluminescence spectra.

QD size / nm (exciton peak energy / wavelength)	Emission origin	Emission peak energy / eV (wavelength / nm)	FWHM / eV
3.1 (3.1 eV / 400 nm)	Exciton	2.96 (419)	0.21
	Trap	2.06 (602)	0.66
3.3 (2.95 eV / 420 nm)	Exciton	2.82 (440)	0.15
	Trap	1.88 (660)	0.60
3.7 (2.82 eV / 440 nm)	Exciton	2.75 (451)	0.14
	Trap	1.84 (675)	0.57
4.3 (2.70 eV / 460 nm)	Exciton	2.63 (471)	0.11
	Trap	1.75 (708)	0.66

From the data in Fig. 4, as the QD size increases, the trap state emission intensity decreases and the band edge emission intensity increases. In order to analyze the influence of the QD size on the emissive trap states, the intensity of the trap state and band edge emission was integrated, respectively, and the integrated band edge emission, i.e. the number of emitted photons, relative to the overall emission was plotted against the inverse of the QD radius in Fig. 5. The results indicate that the proportion of the band edge emission decreases exponentially with an increase in the inverse of the QD radius. This suggests the increase in the emissive trap states against the inverse of the QD radius, i.e. the surface area increase per unit QD volume (the surface area to volume ratio), thereby implying that the emissive trap states most likely originate from the surface states, and that the surface is not well passivated by the oleylamine employed during the non-injection synthesis. We therefore conclude that the density of the surface emissive states increases with the surface area per unit volume.

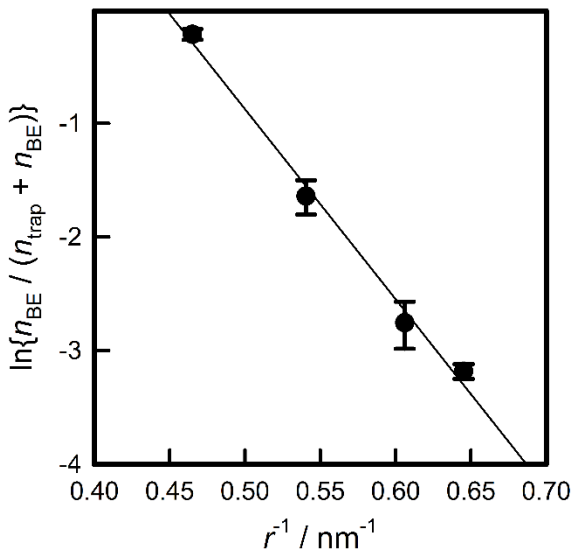

Fig. 5. Integrated CdS QD band edge photoluminescence (n_{BE}) relative to all integrated photoluminescence (n_{BE} + trap state photoluminescence (n_{trap})) plotted against the inverse of the QD radius. The straight line was drawn as a guide.

QD size dependence on photoluminescence dynamics

Time-resolved photoluminescence decays were observed for the synthesized QDs with a diameter of 3.1, 3.3, 3.7 and 4.3 nm. Fig. 6a shows the band edge emission decays. As the QD size increases, the photoluminescence lifetime becomes longer. McLendon et al. reported that the formation rate of a shallow trap state responsible for band edge emission in CdS QDs is <10 ps.[25] Klimov et al. later explained that the hole trapping occur in 1 ps, while an electron is trapped at 20-30 ps.[27, 28] Thus, the photoluminescence data we discuss in the present study most likely originates from charge recombination via localized surface trap states.[31] The inset of Fig. 6a shows the same data, but plotted at the logarithmic scale for the emission intensity axis.

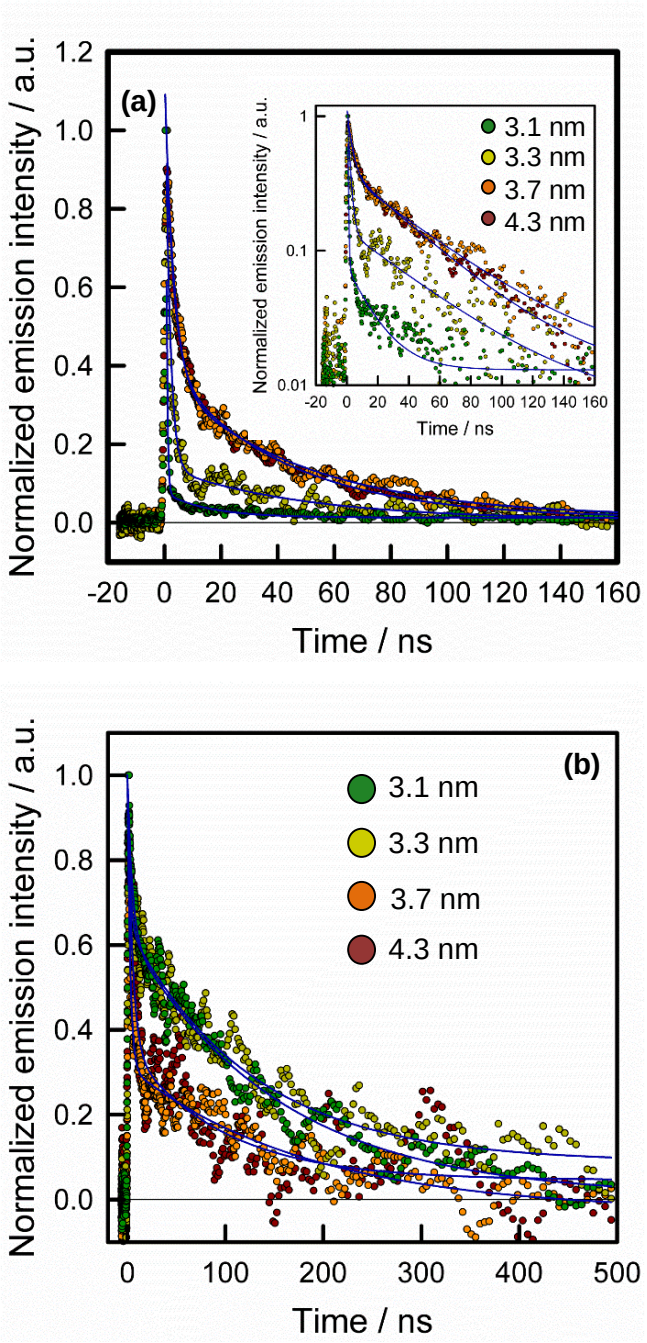

Fig. 6. (a) Transient photoluminescence decays from the exciton states obtained for CdS QD with a diameter of 3.1, 3.3, 3.7 or 4.3 nm, monitored at 420, 435, 450 or 470 nm, respectively. The inset shows as the logarithmic scale for the emission intensity axis. (b) Transient photoluminescence decays from the trap states observed for CdS QD with a diameter of 3.1, 3.3, 3.7 or 4.3 nm, monitored at 600, 650, 650 or 700 nm, respectively. The blue lines were obtained by fitting the decay data with an exponential decay function.

The results clearly indicate that more than one component is involved for the photoluminescence decay from the exciton state. These decay kinetics can be clearly analysed using a bi-exponential decay function as shown in the equation 1, in agreement with the recent studies[45] and in contrast to other kinetic models.[30]

$$I(t) = A_F \exp\left(-t/\tau_F\right) + A_S \exp\left(-t/\tau_S\right) \quad (1)$$

where $I(t)$ is emission intensity at time t, A_F is amplitude of the faster decay component, τ_F is lifetime of the faster decay component, A_S is amplitude of the slower decay component, and τ_S is lifetime of the slower decay component. The fitted results are shown as blue lines in Figure 6a, and are summarized in Table 2. Photoluminescence quantum yields (QYs) from the exciton states were also measured, and added in Table 2. It is clear that the lifetimes of the faster components becomes longer with the QD size increase, and moreover the amplitudes of the slower components increase with the QD size increase. These appear to be associated with the QYs increase. These results are in agreement with the previous reports for CdSe QDs.[48, 49] Chen and co-workers recently reported that bare CdS QDs with 60 % QY produced larger amplitudes of the long lifetime component originating from the radiative recombination of charge carriers in surface states.[45] Jones and Scholes discussed a series of decay times of band edge photoluminescence owing to charge transfer reactions between the exciton and the shallow surface trap states for CdSe QDs.[11, 50, 51] Thus, the slower band edge emission in the present study most likely results from the delayed band edge emission via the shallow surface trap states.

Table 2. Fitted results of transient photoluminescence decays and emission quantum yields (QYs) of various CdS QD sizes.

QD size / nm	Monitored λ / nm	A_F / %	τ_F / ns	A_S / %	τ_S / ns	QY / %
3.1	420	98.3	0.39	1.7	15.9	0.053±0.02
	600	37.6	4.73	62.4	152	5.7±0.03
3.3	435	89.8	1.65	10.2	48.3	0.25±0.03
	650	39.0	2.54	61.0	126	10.8±0.05
3.7	450	69.2	3.20	30.8	49.0	1.1±0.02
	650	66.8	2.79	33.2	183	12.3±0.05
4.3	470	64.8	2.93	35.2	41.6	5.9±0.03
	700	67.2	4.99	32.8	95.6	3.0±0.09

Transient photoluminescence decays from the trap states are shown in Fig. 6b. The bi-exponential fitting results for these decays are shown as dark blue lines in Fig. 6b, and are summarized in Table 2. The decay kinetics was almost independent of the monitored wavelength. Interestingly, relative amplitudes of the faster and slower components are dependent upon the QD size. The faster decay components dominate the kinetics for larger QDs, while the smaller QDs indicate larger amplitudes for the slower component. McLendon et al. reported a formation rate (30 ps) of the deep trap states responsible for surface trap state emission (>570 nm),[25] and explained that the deep trap state forms following shallow trap to trap diffusion. As discussed above, the proportion of emissive trap states increases with the surface area increase per unit QD volume, i.e. QD size decrease. The slower components from Figure 6b must therefore originate from the emission from the deep trap states.

These kinetic results also suggest that the population of the deep trap states increases with the QD size decrease, and thus more photogenerated charges are trapped at the deep surface trap states. The quantum yield of photoluminescence from the surface trap states does not show their relationship with QD size (see Table 2), however the ratio of the trap state photoluminescence to the total photoluminescence quantum yield (QY_{trap}/(QY_{trap} and $QY_{BandEdge}$) decreases with the QD size increase, i.e. 0.99, 0.98, 0.92, and 0.34 for the QD size of 3.1, 3.3, 3.7 and 4.3 nm, respectively, indicating the same relationship as the results shown in Fig. 5 (increase of the emissive trap states as a function of size decrease).

QD surface structure and origin of trap state emission

In order to relate the QD composition to the surface structure, XPS measurements were performed for the synthesized QDs. Previous studies demonstrated that XPS is a reliable technique for distinguishing surface from core atoms for semiconductor QDs.[42, 52-54] XPS spectra of the QDs with various sizes were observed and compared to that of bulk CdS powder. Elemental analysis data are summarized in Table 3. The ratio of Cd to S atoms was determined from the integrated Cd and S signals with appropriate atomic sensitivity factors from the spectrometer. Since the inelastic mean free path of the electrons is similar to the QD diameter, the relative concentration of the detected Cd and S atoms was corrected following the method described in the electronic supplementary information. All of the corrected Cd and S ratios shown in Table 3 indicate a larger number of Cd atoms compared to S atoms in a QD, suggesting that all prepared QDs have enriched Cd surface. This observation is plausible, since a greater amount of Cd precursor was employed during the synthesis process, however the results indicated no clear correlation with QD size.

Table 3. XPS composition analysis of synthesized CdS QDs. Cd_{SV} and S_S indicates Cd component with sulfur vacancy and surface sulfur component, respectively.

QD size / nm	O 1s / %	Cd 3d / %	S 2p / %	Cd/S ratio	Cd/S corrected	Cd_{SV}/ Cd[a] ratio	S_S/S[a] ratio
3.1	25.2 ± 3.0	43.7 ± 3.0	31.1 ± 3.0	1.41	1.28	0.29 ±0.04	0.135
3.3	24.4 ± 1.0	47.0 ± 1.0	28.6 ± 1.0	1.64	1.50	0.155 ±0.02	0.135
3.7	20.9 ± 3.5	47.6 ± 1.0	31.5 ± 3.3	1.51	1.39	0.04± 0.01	0.074
4.3	23.9 ± 1.0	45.9 ± 1.5	30.2 ± 2.0	1.52	1.41	-	-
Bulk	7.7± 1.0	49.1± 1.0	43.2± 1.0	1.14	-	-	-

[a]composition of Cd components with sulfur vacancy, Cd_{SV}, and surface sulfur components, S_S, is obtained from the number of these components divided by the total number of Cd and S atoms in a QD, respectively.

The obtained XPS spectra of Cd 3d and S 2p regions for CdS QDs were compared to those of bulk CdS powder, and analysed with a Voigt function. The results of analysis in the Cd 3d regions are shown in Fig. 7, while analysis in the S 2p regions is shown in Fig. S4. In Fig. 7, the best fit for the bulk CdS XPS peak data was obtained with two peaks at 404.65 and 411.43 eV with Gaussian band widths of 0.75 eV for Cd 3d 5/2 region and 0.74 eV for Cd 3d 3/2 region, and Lorentzian band widths of 0.35 eV

for Cd 3d 5/2 region and 0.34 eV for Cd 3d 3/2 region, respectively. For CdS QDs, fitting was performed, assuming the same line widths as those from the fitting with bulk CdS, however the spectra required at least one more component in each region to obtain reasonable fittings. The fitting results are summarized in Table S2. In addition to the main bands, lower binding energy components appeared at approximately 404.25 eV in Cd 3d 5/2 region and 410.9 eV in Cd 3d 3/2 region. Previous XPS studies of CdS and CdSe QDs identified a higher binding energy component, assigned to surface Cd terminal atoms.[42, 53] In contrast, Umbach et al. observed a lower binding energy component for CdS QDs, and assigned it to Cd segregation with sulfur desorption on the QD surface.[52] In our QD samples, this observation effectively indicates the existence of surface Cd with sulfur vacancy, since the reduced number of electronegative S neighbours results in a lower binding energy shift. Following this explanation, we attribute these lower binding energy components to the signal from surface Cd with sulfur vacancy.

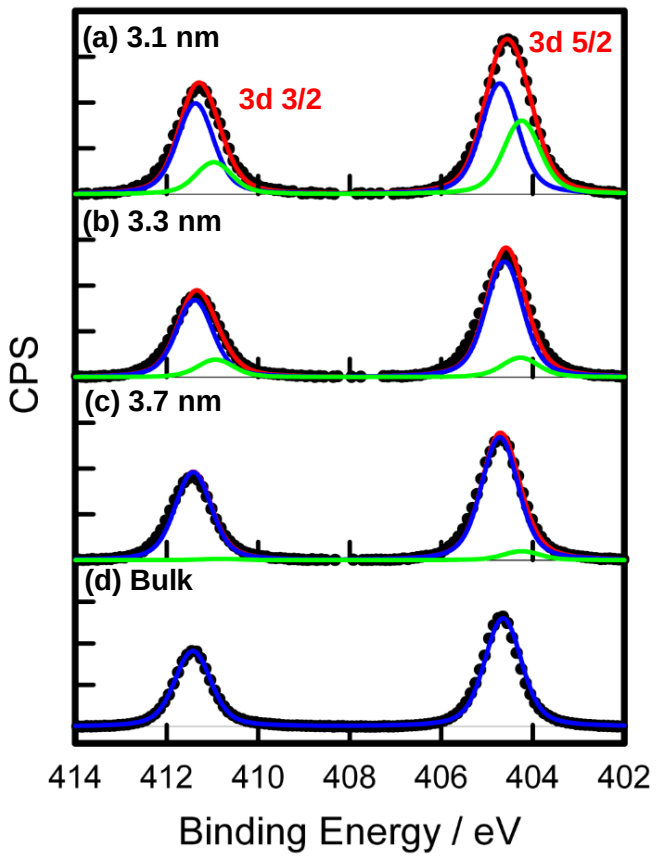

Fig. 7. XPS elemental analysis of Cd 3d regions for CdS QDs with a diameter of (a) 3.1 nm, (b) 3.3 nm and (c) 3.7 nm, and (d) CdS bulk powder. The best fit for bulk CdS XPS peak data was obtained by using a Voigt function with Gaussian band widths of 0.75 eV for Cd 3d 5/2 region and 0.74 eV for Cd 3d 3/2 region, and Lorentzian band widths of 0.35 eV for Cd 3d 5/2 region and 0.34 eV for Cd 3d 3/2 region. For CdS QDs, fitting was performed with the same band width to identify signals from core Cd atoms (higher binding energy) and from surface Cd with sulfur vacancy (lower binding energy). Black dots represent raw XPS data, blue lines represent fits for core Cd atoms, green lines represent fits for surface Cd, and red lines represent convolution of blue and green lines.

The contribution of the signals from surface Cd with sulfur vacancy was analysed from the fitting. The results are summarized in Table 3. Interestingly, the ratio of Cd with sulfur vacancy to total Cd atoms (Cd_{SV}/Cd) becomes smaller with increase in the QD size. Fig. 8 shows this ratio plotted as a function of the inverse of the QD radius. The results indicate that the population of Cd with sulfur vacancy increases exponentially with increase in the inverse of the QD radius. This relationship also suggests that the exponential increase of the Cd with sulphur vacancy sites relates to the QD surface area to volume ratio. Previously, a number of electron trap states located around 0.63~0.7 eV below the conduction band edge was identified using bulk CdS crystals.[55] Such trap states were assigned to sulfur vacancies.[46] Grätzel et al. speculated that the photoluminescence with the peak around 700 nm originated from radiative recombination via the electron trap site at the sulfur vacancy located at 0.63~0.7 eV below the conduction band edge.[29, 56] Our XPS results clearly support these previous assignments that the lower energy wide band emission originates from the electron trap states in surface Cd with sulfur vacancies.

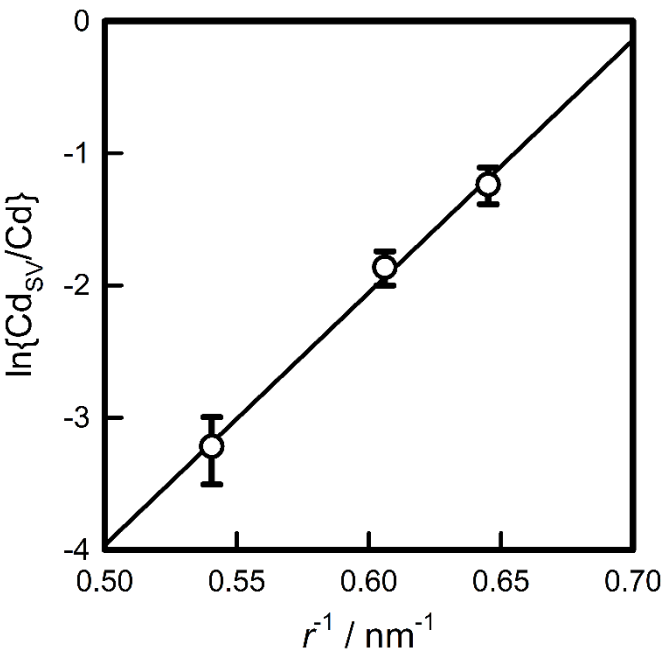

Fig. 8. Ratio of Cd with sulfur vacancy to total Cd atoms (Cd_{SV}/Cd) plotted against the inverse of the QD radius. The straight line was drawn as a guide.

Based on steady state and dynamics photoluminescence studies above, the population of the deep trap states increases with the QD size decrease. From the XPS study, the number of Cd atoms with sulfur vacancy, which act as an electron trap state, increases with the QD size decrease. Therefore, we conclude that the surface deep trap state mainly originates from the electron trap state whose population increases with the QD size decrease.

In contrast to the Cd 3d region, the analysis of the S 2p region indicated higher binding energy components compared to the main bands. These higher binding energy components have been

attributed to the surface sulfur atoms.[42, 57] This observation is plausible, since the decreased electronegativity with S surface atoms indicates a higher binding energy shift. The fitting results and the contribution of these higher energy components to the main bands are shown in Fig. S4 and Table S2, and are summarized in Table 3, respectively. Similar to the observations in the Cd 3d region, the ratio of the surface sulfur components to the total atoms, S_S/S, tends to decrease with the QD size increase, which is associated with the band edge photoluminescence QY increase. Such observations are in agreement with the results reported from Krauss et al.[42] that the sulfur surface terminals of the CdS QD introduce surface trap states creating non-radiative recombination pathways.

Conclusions

Monodisperse CdS QDs with a wide variety of QD size were synthesized by a non-injection method. The QD size could be readily increased by simply increasing reaction temperature and time, while the narrow size distribution was maintained. Following photoluminescence studies, we found that the low energy trap state emission originates from the surface deep trap states, and the proportion of the surface deep trap state emission increases with the QD size decrease. XPS measurements identified the existence of surface Cd with sulfur vacancy sites whose population increases with the QD size decrease. We therefore conclude that the trap state emission mainly originates from the surface deep trapped electrons at the surface Cd with sulfur vacancy sites.

Acknowledgements

We acknowledge Dr. Takao Sakata and Prof. Hirotaro Mori from the Research Center for Ultra-High Voltage Electron Microscopy, Osaka University, Japan, and Dr. Phil Francis and Prof. Dougal G McCulloch, RMIT Microscopy & Microanalysis Facility, School of Applied Sciences, RMIT University, Australia, for TEM measurements. We thank Dr. Matthew Field, RMIT Microscopy & Microanalysis Facility, School of Applied Sciences, RMIT University, for XPS measurements. This work was financially supported by the JST PRESTO program (Photoenergy Conversion Systems and Materials for the Next Generation Solar Cells) and Grant-in-Aid for Scientific Research, 21550133, from the Ministry of Education, Culture, Sports, Science and Technology, Japan. We also acknowledge support from a LIEF program (LE140100104), the Australian Research Council, Australia. T. S. acknowledges internship support from Deutscher Akademischer Austausch Dienst (DAAD), RISE worldwide program, Germany. Platform Technologies Research Institute (PTRI) at RMIT University is also acknowledged.

Notes and references

[a] School of Aerospace, Mechanical and Manufacturing Engineering, RMIT University, Bundoora, VIC 3083, Australia.
[b] School of Applied Sciences, RMIT University, Melbourne, VIC 3001, Australia.
[c] Research Core for Interdisciplinary Sciences, Okayama University, 3-1-1 Tsushimanaka, Okayama, Okayama 700-8530, Japan.
[d] Institute for Chemical Research, Kyoto University, Gokasho, Uji, Kyoto 611-0011, Japan
[e] Office for University-Industry Collaboration, Osaka University, 2-1 Yamada-oka, Suita, Osaka 565-0871, Japan
[f] Japan Science and Technology Agency (JST), PRESTO, 4-1-8 Honcho Kawaguchi, Saitama 332-0012, Japan
† Current address: PC Department, Fritz-Haber-Institut der Max-Planck-Gesellschaft, Faradayweg 4-6, 14195 Berlin, Germany.

Corresponding Author
Tel: +61 (0)3 9925 6127; Fax: +61 (0)3 9925 6139
*E-mail: yasuhiro.tachibana@rmit.edu.au; y.tachibana@uic.osaka-u.ac.jp

Electronic Supplementary Information (ESI) available: Absorption spectra of CdS QDs obtained by employing a different precursor, ligand and/or solvent, TEM measurements of CdS QDs with a series of sizes, sensitivity calibration for XPS elemental analysis, and XPS analysis of S 2p regions. See DOI: 10.1039/b000000x/

1. T. V. Duncan, M. A. Mendez Polanco, Y. Kim and S.-J. Park, *J. Phys. Chem. C*, 2009, **113**, 7561-7566.
2. A. Hassinen, I. Moreels, K. De Nolf, P. F. Smet, J. C. Martins and Z. Hens, *J. Am. Chem. Soc.*, 2012, **134**, 20705-20712.
3. A. Aharoni, T. Mokari, I. Popov and U. Banin, *J. Am. Chem. Soc.*, 2006, **128**, 257-264.
4. M. A. Hines and G. D. Scholes, *Adv. Mater.*, 2003, **15**, 1844-1849.
5. J. M. Pietryga, R. D. Schaller, D. Werder, M. H. Stewart, V. I. Klimov and J. A. Hollingsworth, *J. Am. Chem. Soc.*, 2004, **126**, 11752-11753.
6. J. van Embden, K. Latham, N. W. Duffy and Y. Tachibana, *J. Am. Chem. Soc.*, 2013, **135**, 11562-11571.
7. A. P. Alivisatos, *Science (New York, N.Y.)*, 1996, **271**, 933-937.
8. A. M. Smith and S. Nie, *Acc. Chem. Res.*, 2010, **43**, 190-200.
9. J. Jasieniak, M. Califano and S. E. Watkins, *ACS Nano*, 2011, **5**, 5888-5902.
10. U. Banin, Y. Cao, D. Katz and O. Millo, *Nature*, 1999, **400**, 542-544.
11. M. Jones and G. D. Scholes, *J. Mater. Chem.*, 2010, **20**, 3533-3538.
12. V. I. Klimov, D. W. McBranch, C. A. Leatherdale and M. G. Bawendi, *Phys. Rev. B Condens. Matter Mater. Phys.*, 1999, **60**, 13740-13749.
13. A. C. Carter, C. E. Bouldin, K. M. Kemner, M. I. Bell, J. C. Woicik and S. A. Majetich, *Phys. Rev. B: Condens. Matter*, 1997, **55**, 13822-13828.
14. Y. Tachibana, K. Umekita, Y. Otsuka and S. Kuwabata, *J. Phys. Chem. C*, 2009, **113**, 6852-6858.
15. J. Zheng, X. Yuan, M. Ikezawa, P. Jing, X. Liu, Z. Zheng, X. Kong, J. Zhao and Y. Masumoto, *J. Phys. Chem. C*, 2009, **113**, 16969-16974.
16. W. Nan, Y. Niu, H. Qin, F. Cui, Y. Yang, R. Lai, W. Lin and X. Peng, *J. Am. Chem. Soc.*, 2012, **134**, 19685-19693.
17. Q. Zeng, X. Kong, Y. Sun, Y. Zhang, L. Tu, J. Zhao and H. Zhang, *J. Phys. Chem. C*, 2008, **112**, 8587-8593.
18. J. Sun, J. Zhao and Y. Masumoto, *Appl. Phys. Lett.*, 2013, **102**, 053119/053111-053119/053114.
19. Y. Tachibana, H. Y. Akiyama, Y. Ohtsuka, T. Torimoto and S. Kuwabata, *Chem. Lett.*, 2007, **36**, 88-89.

20. Y. Tachibana, K. Umekita, Y. Otsuka and S. Kuwabata, *J. Phys. D Appl. Phys.*, 2008, **41**, 102002/102001-102002/102005.
21. C. B. Murray, D. J. Norris and M. G. Bawendi, *J. Am. Chem. Soc.*, 1993, **115**, 8706-8715.
22. X. Peng, J. Wickham and A. P. Alivisatos, *J. Am. Chem. Soc.*, 1998, **120**, 5343-5344.
23. W. W. Yu and X. Peng, *Angew. Chem., Int. Ed.*, 2002, **41**, 2368-2371.
24. L. Spanhel, M. Haase, H. Weller and A. Henglein, *J. Am. Chem. Soc.*, 1987, **109**, 5649-5655.
25. M. O'Neil, J. Marohn and G. McLendon, *Chem. Phys. Lett.*, 1990, **168**, 208-210.
26. N. Chestnoy, T. D. Harris, R. Hull and L. E. Brus, *J. Phys. Chem.*, 1986, **90**, 3393-3399.
27. V. I. Klimov, P. Haring-Bolivar, H. Kurz and V. A. Karavanskii, *Superlattices Microstruct.*, 1996, **20**, 395-404.
28. V. Klimov, P. H. Bolivar and H. Kurz, *Phys. Rev. B: Condens. Matter*, 1996, **53**, 1463-1467.
29. J. J. Ramsden and M. Grätzel, *J. Chem. Soc., Faraday Trans. 1*, 1984, **80**, 919-933.
30. M. O'Neil, J. Marohn and G. McLendon, *J. Phys. Chem.*, 1990, **94**, 4356-4363.
31. A. Hässelbarth, A. Eychmüller and H. Weller, *Chem. Phys. Lett.*, 1993, **203**, 271-276.
32. M. Kanehara, H. Arakawa, T. Honda, M. Saruyama and T. Teranishi, *Chem. - Eur. J.*, 2012, **18**, 9230-9238, S9230/9231-S9230/9234.
33. W. W. Yu, L. Qu, W. Guo and X. Peng, *Chem. Mater.*, 2003, **15**, 2854-2860.
34. F. Wu, J. Z. Zhang, R. Kho and R. K. Mehra, *Chem. Phys. Lett.*, 2000, **330**, 237-242.
35. N. Pradhan and S. Efrima, *J. Am. Chem. Soc.*, 2003, **125**, 2050-2051.
36. P. S. Nair, T. Radhakrishnan, N. Revaprasadu, G. Kolawole and P. O'Brien, *J. Mater. Chem.*, 2002, **12**, 2722-2725.
37. M. A. Malik, N. Revaprasadu and P. O'Brien, *Chem. Mater.*, 2001, **13**, 913-920.
38. Y. W. Jun, S. M. Lee, N. J. Kang and J. Cheon, *J. Am. Chem. Soc.*, 2001, **123**, 5150-5151.
39. Y. C. Cao and J. Wang, *J. Am. Chem. Soc.*, 2004, **126**, 14336-14337.
40. J. Ouyang, J. Kuijper, S. Brot, D. Kingston, X. Wu, D. M. Leek, M. Z. Hu, J. A. Ripmeester and K. Yu, *J. Phys. Chem. C*, 2009, **113**, 7579-7593.
41. A. Aboulaich, D. Billaud, M. Abyan, L. Balan, J.-J. Gaumet, G. Medjadhi, J. Ghanbaja and R. Schneider, *ACS Appl. Mater. Interfaces*, 2012, **4**, 2561-2569.
42. H. H.-Y. Wei, C. M. Evans, B. D. Swartz, A. J. Neukirch, J. Young, O. V. Prezhdo and T. D. Krauss, *Nano Lett.*, 2012, **12**, 4465-4471.
43. J. H. Warner, S. Djouahra and R. D. Tilley, *Nanotechnology*, 2006, **17**, 3035-3038.
44. Z. Y. Pan, X. J. Liu, S. Y. Zhang, G. J. Shen, L. G. Zhang, Z. H. Lu and J. Z. Liu, *J. Phys. Chem. B*, 1997, **101**, 9703-9709.
45. H.-L. Chou, C.-H. Tseng, K. C. Pillai, B.-J. Hwang and L.-Y. Chen, *J. Phys. Chem. C*, 2011, **115**, 20856-20863.
46. A. A. Vuylsteke and Y. T. Sihvonen, *Phys. Rev.*, 1959, **113**, 40-42.
47. C. C. Yang and S. Li, *J. Phys. Chem. C*, 2008, **112**, 2851-2856.
48. X. Wang, L. Qu, J. Zhang, X. Peng and M. Xiao, *Nano Lett.*, 2003, **3**, 1103-1106.
49. G. Schlegel, J. Bohnenberger, I. Potapova and A. Mews, *Phys. Rev. Lett.*, 2002, **88**, 137401/137401-137401/137404.
50. M. Jones, S. Lo Shun and G. D. Scholes, *Proc. Natl. Acad. Sci. U. S. A.*, 2009, **106**, 3011-3016.
51. M. Jones, S. S. Lo and G. D. Scholes, *J. Phys. Chem. C*, 2009, **113**, 18632-18642.
52. U. Winkler, D. Eich, Z. H. Chen, R. Fink, S. K. Kulkarni and E. Umbach, *Phys. Status Solidi A*, 1999, **173**, 253-259.
53. J. Jasieniak and P. Mulvaney, *J. Am. Chem. Soc.*, 2007, **129**, 2841-2848.
54. J. E. B. Katari, V. L. Colvin and A. P. Alivisatos, *J. Phys. Chem.*, 1994, **98**, 4109-4117.
55. K. H. Nicholas and J. Woods, *Br. J. Appl. Phys.*, 1964, **15**, 783-795.
56. J. J. Ramsden, S. E. Webber and M. Grätzel, *J. Phys. Chem.*, 1985, **89**, 2740-2743.
57. U. Winkler, D. Eich, Z. H. Chen, R. Fink, S. K. Kulkarni and E. Umbach, *Chem. Phys. Lett.*, 1999, **306**, 95-102.